Epithelial NCAPD3 expression protects against stress-induced intestinal injury in mice

Isabel Johnston[1], Erin E. Johnson[1,2], Afshin Khan[1], Michelle S. Longworth[1,3], & Christine McDonald[1,3*]

[1]Department of Inflammation & Immunity, Cleveland Clinic Research, Cleveland Clinic, Cleveland, Ohio, United States of America

[2]Department of Biology, John Carroll University, University Heights, Ohio, United States of America

[3]Department of Molecular Medicine, Cleveland Clinic Lerner College of Medicine at Case Western Reserve University, Cleveland, Ohio, United States of America

* Corresponding author

E-mail: mcdonac2@ccf.org (CM)

Short Title: NCAPD3 protects intestinal homeostasis during stress

Key Words: condensin, ulcerative colitis, epithelial barrier, mouse model, intestinal homeostasis

Abstract

Intestinal epithelial cells are central players in mucosal barrier integrity and host-microbe interactions. Genetic studies have revealed that epithelial dysfunction is a key contributor to the pathogenesis of inflammatory bowel disease. Non-SMC condensin II complex subunit D3 (NCAPD3) is essential for chromatin organization and stability. NCAPD3 also promotes antimicrobial defense and autophagy responses *in vitro*. NCAPD3 expression is decreased in intestinal epithelial cells from patients with ulcerative colitis; however, it is not known whether loss of NCAPD3 expression drives intestinal barrier dysfunction or is a result of disease-associated inflammation. To investigate this relationship *in vivo*, a tissue-specific approach was required, as global constitutive knockout of NCAPD3 is embryonic lethal. Therefore, a transgenic mouse line with doxycycline-inducible expression of a short hairpin RNA targeting NCAPD3 restricted to villin-expressing cells was generated (NCAPD3KD mice) to enable the study of NCAPD3 function in the intestinal epithelium. Treatment of NCAPD3KD mice with 9-tert-butyl doxycycline resulted in ~75% reduction of NCAPD3 protein in $EpCAM^+$ intestinal cells. Short-term epithelial NCAPD3 knockdown did not induce spontaneous colitis but was associated with increased serum amyloid A and a trend towards increased intestinal permeability. Upon dextran sodium sulfate or *Salmonella enterica* serovar Typhimurium ΔAroA challenge, NCAPD3KD mice exhibited exacerbated weight loss, higher disease activity, increased histopathological damage, abnormal colonic cytokines and chemokines, and significantly increased intestinal permeability. These results indicate that NCAPD3 expression in the intestinal epithelium is required for optimal barrier maintenance and antimicrobial defense under chemical or microbial stress. These findings support prior *in vitro* observations and solidify NCAPD3 as a regulator of intestinal epithelial barrier function and mucosal host defense.

Author Summary

NCAPD3 is a multifunctional protein with established roles in chromatin organization, genome stability, mitochondrial function, and antimicrobial defense. Dysregulated NCAPD3 is implicated in human diseases, such as inflammatory bowel disease (IBD) and microcephaly; however, due to its essential role in cellular division, determination of whether NCAPD3 loss drives these pathologies *in vivo* has been lacking. Using a new transgenic mouse model that selectively reduces NCAPD3 expression in intestinal epithelial cells, our study

51 establishes NCAPD3 as an epithelial regulator of the mammalian intestine that enhances epithelial barrier
52 resilience and antimicrobial defense during stress. Although dispensable for short-term basal homeostasis,
53 NCAPD3 function becomes critical during epithelial injury and enteric infection. Reduced NCAPD3 expression
54 may therefore lower the threshold for inflammatory disease by weakening barrier integrity, amplifying
55 inflammatory cascades, and impairing antimicrobial defenses. These findings position NCAPD3 as a potential
56 modulator of IBD susceptibility and highlight chromatin organization as an important, previously
57 underappreciated layer of intestinal epithelial regulation.
58

59 **Introduction**

60 The intestinal epithelium is a vital single-cell barrier between the host and the external environment, consisting
61 of a diverse range of specialized intestinal epithelial cells (IECs) (1). This dynamic interface allows the absorption
62 of nutrients and fluids, provides innate immune defenses, and helps maintain a homeostatic balance with the gut
63 microbiota (2). The epithelium provides a physical barrier, with intercellular tight junctions responsible for
64 maintaining a seal between adjacent cells (3). Additionally, IECs convey signals to mucosal immune cells and
65 help coordinate differential immune responses to commensal and pathogenic bacteria. Defects in epithelial
66 barrier integrity are a hallmark of inflammatory bowel diseases (IBD), such as ulcerative colitis (UC) and Crohn's
67 disease (CD), and render the host susceptible to enteric infections (2).

68 In the context of IBD, disruption and dysregulation of IEC function are key drivers of chronic intestinal
69 inflammation (4). Defects in epithelial barrier integrity, including altered tight junction architecture, impaired
70 mucus production, and reduced antimicrobial peptide secretion, lead to increased intestinal permeability and
71 inappropriate exposure of the mucosal immune system to luminal microbes and antigens. Increased exposure
72 of the host tissues to microbial products, from a so-called "leaky gut", leads to chronic inflammation. Beyond
73 barrier failure, IECs in IBD display aberrant innate immune signaling, stress responses, and altered interactions
74 with the microbiota, all of which contribute to sustained inflammatory responses characteristic of IBD.
75 Importantly, IBD has a clear genetic component, with genome-wide association studies identifying over 250 risk
76 loci, many of which are directly linked to epithelial cell function (5). Collectively, these findings highlight IECs as

77 central regulators of intestinal homeostasis and underscore how IEC dysfunction can predispose individuals to
78 IBD.

79 Non-SMC condensin II complex subunit D3 (NCAPD3) is a core component of the condensin II complex,
80 which promotes chromatin condensation during mitotic initiation (6) and maintains genomic stability (7). Beyond
81 its canonical nuclear functions, NCAPD3 has been implicated in retrotransposon silencing (8), mitochondrial
82 redox (9), and antimicrobial defenses (10, 11). Consequently, the dysregulation of NCAPD3 has been associated
83 with multiple human pathologies. Loss-of-function mutations drive microcephaly (12), while overexpression has
84 been associated with cancer progression (13-19). Critically, reduced NCAPD3 expression has been observed
85 in intestinal epithelial cells isolated from UC patients (11). However, despite evidence from cell-based and *ex*
86 *vivo* analyses of intestinal epithelial cells, the role of NCAPD3 in maintaining intestinal epithelial homeostasis *in*
87 *vivo* remains uncharacterized. Specifically, it is unclear how loss or dysregulation of NCAPD3 affects epithelial
88 integrity or susceptibility to intestinal inflammation within an organismal context.

89 To directly define the role of NCAPD3 in the intestinal epithelium *in vivo*, we created an inducible,
90 intestinal epithelial cell-specific NCAPD3 knockdown mouse model. Using this model, we examined whether
91 epithelial NCAPD3 is necessary to maintain intestinal homeostasis or to protect the intestinal barrier during
92 inflammatory or infectious challenges. Specifically, we assessed the effects of NCAPD3 depletion on intestinal
93 permeability, susceptibility to chemically induced epithelial injury, and host defense against enteric bacterial
94 infection. Our studies provide evidence that NCAPD3 expression in the intestinal epithelium is essential for
95 optimal barrier integrity and antimicrobial defense under stress from chemical or microbial challenges. These
96 findings underscore the important role of NCAPD3 in maintaining intestinal health.

97

98 **Results**

99 **Development of an intestinal epithelial cell-specific inducible NCAPD3 knockdown murine line.** To
100 investigate the role of NCAPD3 in the murine intestinal epithelium, we designed mice with inducible expression
101 of a shRNA targeting NCAPD3 restricted to villin-expressing cells. Candidate shRNA sequences were screened
102 for NCAPD3 knockdown efficiency prior to the creation of the knock-in transgene cassette (**Fig. S1A & Table**
103 **S1**). The shRNA sequence targeting the 3' untranslated region that reproducibly reduced NCAPD3 levels over

104 50% was used for the knock-in cassette. A CRISPR/Cas9-mediated targeted integration strategy of the
105 transgene cassette into the *Col1a1* safe harbor locus was used to minimize the potential impact of the knock-in
106 on the expression of other genes (**Fig. 1A**). Three injection conditions with different ratios of Cas9/small guide
107 RNA/targeting vector were used to create targeted B6SJL/F2 fertilized oocytes that were then transferred to CD1
108 pseudo-pregnant recipients. The resulting 78 pups (founders) were then screened by qPCR and confirmed by
109 sequencing of PCR products for transgene insertion and orientation (**Fig. S1B**). Transgene insertion was
110 detected in 25.6% of the founders, and 85% of the transgenes were inserted in the correct orientation (21.8%
111 overall). Of the mice with correctly oriented transgenes, germline transmission occurred in 40% of the lines.

112 Induction of transgene cassette expression and knockdown of NCAPD3 protein in intestinal epithelial
113 cells in response to a non-antimicrobial tetracycline analogue, 9-TB-Dox (20), was evaluated by fluorescent
114 imaging, immunostaining, and immunoblot analyses. As the microbiota contributes to intestinal health, 9-TB-Dox
115 was used to activate expression of the NCAPD3-targeting shRNA and GFP reporter gene instead of the antibiotic
116 tetracycline or doxycycline to minimize the impact of the inducing agent on the microbiota. After 4 days of daily
117 9-TB-Dox i.p. administration, gross evaluation of tissues by fluorescent imaging confirmed selective expression
118 of the GFP reporter gene throughout the small intestine, cecum, and colon (**Fig. 1B**). Examination of
119 extraintestinal tissues also known to express villin, such as the pancreas and kidney, had low level GFP
120 expression; however, fluorescence levels in these tissues were approximately 50-fold lower than those observed
121 in the intestine.

122 Closer evaluation of intestinal tissue by confocal fluorescent microscopy showed epithelial-specific GFP
123 expression after 9-TB-Dox treatment (**Fig. 1C & 1D**). NCAPD3 immunostaining of the same tissue section
124 revealed broad NCAPD3 expression in all cells of control mice and decreased NCAPD3 staining intensity in the
125 GFP-positive epithelium of 9-TB-Dox-treated mice. GFP expression varied along the crypt axis with lower/no
126 expression in the crypt base and strong expression closer to the crypt tip, mirroring reported increased
127 expression of villin as epithelial cells differentiate (21). Importantly, the GFP and NCAPD3 staining did not
128 overlap, indicating effective knockdown in shRNA-expressing cells. To more directly assess the degree of
129 NCAPD3 knockdown in intestinal epithelial cells after transgene induction, flow-sorted colonic $EpCAM^+$/ $CD45^-$/
130 GFP^+ cells from 9-TB-Dox mice were compared to $EpCAM^+$/ $CD45^-$ cells from control mice. Immunoblot analysis

131 of NCAPD3 protein levels revealed a marked reduction (75%) in intestinal epithelial cells from 9-TB-Dox treated
132 mice (**Fig. 1E**). These data demonstrate the successful genetic engineering of mice to create an inducible,
133 intestinal epithelial cell-specific knockdown of NCAPD3 expression to facilitate the *in vivo* evaluation of the role
134 of NCAPD3 in the intestinal epithelium.
135
136 **Short term NCAPD3 knockdown in the intestinal epithelium is not sufficient to induce spontaneous**
137 **colitis.** To assess the direct impact of reduced NCAPD3 expression in intestinal epithelial cells *in vivo*,
138 NCAPD3KD mice were treated daily with 9-TB-Dox or saline for 10 days. Although 9-TB-Dox-treated mice tended
139 to lose more weight than control animals, no significant differences in weight loss, gross colonic appearance, or
140 colon length were observed (**Fig. 2A & 2B**). Colonic tissue histopathology evaluation using a standardized colitis
141 scoring system did not identify signs of intestinal inflammation in any animal (**Fig. 2C**). Intestinal permeability
142 was assessed using a flagellin bioassay on endpoint plasma samples and showed a trend of increased
143 permeability in NCAPD3KD mice treated with 9-TB-Dox (**Fig. 2D**). In addition, 9-TB-Dox treated NCAPD3KD
144 mice had 2.1 fold increased levels of the systemic acute phase marker of inflammation, SAA relative to control
145 mice (**Fig. 2E**). Overall, these data indicate that short term NCAPD3 knockdown in the intestinal epithelium is
146 not sufficient to induce spontaneous colitis but appears to mildly elevate basal inflammation and gut
147 permeability.
148
149 **Epithelial NCAPD3 knockdown increases sensitivity to intestinal damage induced by DSS.** To further
150 investigate the role of NCAPD3 in intestinal barrier maintenance, NCAPD3KD mice were treated with or without
151 9-TB-Dox and administered low-dose DSS for 7 days to induce mild intestinal injury. NCAPD3KD mice treated
152 with 9-TB-Dox lost more weight (**Fig. 3A**) and had a higher DAI (**Fig. 3B & Table S2**) than saline-treated controls.
153 Quantification of colonic tissue histopathology revealed increased colitis in 9-TB-Dox-treated mice (**Fig. 3C &**
154 **Table S3**), driven primarily by increased epithelial damage scores (2.17 saline vs. 2.80 9-TB-Dox; p=0.02).
155 Correlating with increased inflammation and intestinal epithelium damage were increased levels of the
156 proinflammatory chemokines, MIP1α/CCL3 and MIP2/CXCL2, as well as pro-inflammatory, epithelial damaging
157 cytokines, IL-9, IL-15, and IL-17, in colonic tissue samples (**Fig. S3**). Intestinal permeability of 9-TB-Dox treated

158 mice was approximately double that of control mice, as measured by 4 kDa FITC-dextran transit to the blood
159 after oral challenge (**Fig. 3D**) and by flagellin bioassay of endpoint plasma samples (**Fig. 3E**). Endpoint SAA
160 levels were also dramatically elevated 3.8-fold in 9-TB-Dox mice relative to controls (**Fig. 3F**). These results
161 indicate that reduced NCAPD3 expression in intestinal epithelial cells sensitizes mice to intestinal injury by the
162 chemical irritant DSS.
163
164 **NCAPD3 expression strengthens epithelial defense against the diarrheal pathogen *Salmonella*.** Our prior
165 studies in human intestinal epithelial cell culture and *Drosophila* model systems demonstrated a role for NCAPD3
166 in the upregulation of antimicrobial defenses in response to bacterial pathogen challenge (10, 11). Therefore,
167 we examined the impact of NCAPD3 knockdown on the resistance of mice to oral challenge with the diarrheal
168 pathogen *Salmonella enterica serovar* Typhimurium. As infection of C57BL/6 mice with wild-type *S*. Typhimurium
169 results in acute systemic typhoid disease, we used the attenuated ΔAroA strain to cause a chronic enteric
170 infection to better replicate human diarrheal disease (22).
171 First, we characterized the impact of 9-TB-Dox on the growth and survival of *Salmonella* ΔAroA. Using
172 an *in vitro* growth assay, we compared the bactericidal activity of 9-TB-Dox to doxycycline (**Fig. S4A**). After 20
173 hours, doxycycline induced a dose-dependent decrease in *Salmonella* growth, while 9-TB-Dox had no effect. In
174 contrast, a pilot mouse *Salmonella* ΔAroA infection of WT C57BL/6 mice treated with or without 9-TB-Dox
175 showed no differences in fecal bacterial shedding, but increased colonization of cecum and colon tissues (**Fig.**
176 **S4B-D)**. Therefore, we modified our original experimental design to treat all mice with 9-TB-Dox and compare
177 NCAPD3KD mice (KD) with founder mice lacking the rtTA driver required for induction of the transgene cassette
178 (control; C) in the *Salmonella* ΔAroA oral infection model.
179 All mice were pre-treated with 9-TB-Dox, then orally challenged with *Salmonella* ΔAroA, and monitored
180 for 7 days post-infection. Weight loss post-infection and fecal *Salmonella* shedding were moderately higher in
181 KD mice (**Fig. 4A & 4B**). However, no differences were observed in the tissue levels of viable *Salmonella* in the
182 cecum, colon, mesenteric lymph nodes, liver, or spleen (**Fig. 4B**). Epithelial knockdown of NCAPD3 resulted in
183 increased gross colonic damage quantified by a diarrheal scoring system (**Fig. 4C & Table S4**). Further
184 examination of intestinal tissues revealed increased histopathology scores in both the cecum and colon of KD

185 mice (**Fig. 4D & Table S5**). The increased tissue damage correlated with diminished expression of the
186 antimicrobial peptides Reg3β and defensin-β14 (DEFB14) in KD mice (**Fig. 4E**). Together, this shows a role for
187 NCAPD3 in maintenance of intestinal homeostasis during enteric *Salmonella* infection.
188

189 **Discussion**

190 In this study, we generated and validated a novel inducible, intestinal epithelial cell-specific NCAPD3 knockdown
191 mouse model and used it to investigate the *in vivo* role of NCAPD3 in intestinal barrier homeostasis. Using a
192 villin-rtTA driven shRNA system targeted to the Col1a1 safe harbor locus, we achieved robust epithelial-specific
193 reduction of NCAPD3 following induction with the non-antimicrobial tetracycline analogue 9-TB-Dox. This *in vivo*
194 mammalian model enables mechanistic investigation of the observation that UC patients have reduced NCAPD3
195 expression specifically in intestinal epithelial cells (11). Our data support the interpretation that this epithelial
196 NCAPD3 reduction is not a secondary consequence of inflammation but may contribute to epithelial dysfunction
197 and disease pathogenesis.

198 Despite efficient (~75%) epithelial knockdown over 10 days, NCAPD3KD mice did not develop
199 spontaneous colitis. However, the trend toward increased intestinal permeability, elevated circulating flagellin
200 levels, and significantly increased SAA suggest that NCAPD3 loss subtly compromises epithelial barrier integrity,
201 even in the absence of overt histological inflammation. Increased intestinal permeability is increasingly
202 recognized as an early event in IBD, detectable even in quiescent disease and in individuals prior to clinical
203 onset (23-25). The observation that NCAPD3KD mice exhibit low-level permeability and systemic inflammation
204 without visible tissue injury supports the concept that NCAPD3 loss can contribute to epithelial barrier weakening
205 and predispose one to inflammatory conditions. While this study examined only short-term knockdown, chronic
206 NCAPD3 deficiency may exacerbate this basal inflammatory tone and potentially lead to spontaneous disease.
207 Extended knockdown studies will be required to determine whether long-term NCAPD3 reduction alone is
208 sufficient to break the intestinal barrier and drive intestinal pathology.

209 The increase in SAA in NCAPD3KD mice, even at baseline, is notable. SAA is not merely a marker of
210 inflammation but an active participant in inflammatory processes, capable of inducing cytokine production,
211 recruiting immune cells, and contributing to tissue repair responses (26). In this context, elevated SAA in the

212 absence of overt injury may reflect ongoing low-level epithelial stress and induction of repair mechanisms
213 triggered by a subtle compromise to the barrier. Importantly, SAA levels were further amplified following DSS
214 exposure, consistent with an exaggerated systemic response when the compromised epithelium encounters an
215 additional insult.

216 When challenged with DSS or an enteric *Salmonella* infection, NCAPD3KD mice exhibited significantly
217 heightened disease activity, epithelial damage, inflammatory cytokine production, and intestinal permeability
218 compared to controls. The amplification of permeability and inflammation in these settings aligns with the widely
219 proposed "two-hit hypothesis" for IBD pathogenesis, where a genetically predisposed individual may have
220 epithelial vulnerability and mild barrier dysfunction that, when coupled with environmental triggers, can lead to
221 an uncontrolled inflammatory state (27). In this context, reduced NCAPD3 expression may represent a
222 susceptibility factor that does not independently cause disease but sensitizes the host to secondary insults.

223 During DSS-induced injury, NCAPD3 deficiency was associated with significantly increased epithelial
224 damage and elevation in the proinflammatory mediators MIP1α/CCL3, MIP2/CXCL2, IL-9, IL-15, and IL-17. IL-
225 17 and IL-15 are well-established contributors to mucosal inflammation in both DSS colitis and human IBD,
226 promoting leukocyte recruitment and sustaining immune activation (28). Notably, MIP1α/CCL3 and MIP2/CXCL2
227 are key chemokines in IBD that promote the recruitment of macrophages and neutrophils, respectively, and their
228 upregulation correlates with disease severity (29). Whilst it remains unclear whether these changes reflect direct
229 transcriptional dysregulation resulting from NCAPD3 loss or are secondary to increased epithelial damage and
230 permeability, this data suggests that NCAPD3 plays a role in restraining inflammatory amplification following
231 barrier disruption. Further studies are required to determine whether this occurs through direct chromatin-
232 mediated regulation of inflammatory gene programs or indirectly because of worsened epithelial injury.

233 Consistent with our prior *in vitro* and *Drosophila* studies, epithelial NCAPD3 knockdown compromised
234 host defense during *Salmonella* infection. Although tissue bacterial burdens were comparable, NCAPD3KD mice
235 exhibited increased diarrheal severity and worsened histopathology. This was accompanied by reduced
236 expression of the antimicrobial peptides Reg3β and DEFB14. Reg3β is strongly induced during a *Salmonella*
237 enteric infection and contributes to maintaining a distance between luminal bacteria and the epithelial surface
238 (30), while β-defensins directly limit bacterial growth and shape microbiota composition (31). Deficits in

239 antimicrobial peptide production also have implications for IBD, as antimicrobial peptide levels can be reduced
240 even in the presence of pro-inflammatory signaling that typically upregulates their expression (32). As prior
241 enteric infections are known to increase IBD risk in genetically predisposed individuals (33), heightened tissue
242 damage during infection in the setting of reduced NCAPD3 may represent another mechanism linking epithelial
243 chromatin dysregulation to chronic inflammatory susceptibility.

244 Recent advances have highlighted broader roles for chromatin regulators in controlling transcriptional
245 programs governing epithelial differentiation and innate immunity (34). For example, the chromatin architectural
246 protein CTCF, together with cohesin, organizes higher-order chromatin looping at inflammatory cytokine loci and
247 directly regulates transcriptional responses (35, 36). Similarly, SATB1 acts as a genome organizer in immune
248 cells, controlling the expression of cytokines and other immune genes by regulating long-range chromatin
249 interactions (37, 38). NCAPD3 also contributes to genomic stability by repressing retrotransposons and limiting
250 apoptosis (8, 39). Loss of this function can increase DNA damage and cell stress, potentially weakening epithelial
251 turnover and barrier integrity. These examples demonstrate how disruption of chromatin-organizing systems can
252 reprogram inflammatory, stress-response, and differentiation pathways, indicating mechanisms by which
253 dampened levels of NCAPD3 could reshape epithelial function through skewing expression of cytokines,
254 antimicrobial peptides, or junctional proteins.

255 In summary, our study establishes NCAPD3 as an epithelial regulator of the mammalian intestine that
256 enhances epithelial barrier resilience and antimicrobial defense during stress. Although dispensable for short-
257 term basal homeostasis, NCAPD3 function becomes critical during epithelial injury and enteric infection.
258 Reduced NCAPD3 expression may therefore lower the threshold for inflammatory disease by weakening barrier
259 integrity, amplifying inflammatory cascades, and impairing antimicrobial defenses. These findings position
260 NCAPD3 as a potential modulator of IBD susceptibility and highlight chromatin organization as an important,
261 previously underappreciated layer of intestinal epithelial regulation.

262

263 **Materials and Methods**

264 *NCAPD3 KD transgenic mouse line generation*

265 All animal experiments were conducted in accordance with institutional and national guidelines. Animal use
266 protocols were reviewed and approved by the Institutional Animal Care and Use Committees (IACUC) of
267 Cleveland Clinic and Case Western Reserve University. The genetic manipulation of mice was reviewed and
268 approved by the Institutional Biosafety Committee (IBC) of Case Western Reserve University. Experiments were
269 conducted following the ARRIVE guidelines.

270 Short hairpin RNA (shRNA) sequences targeting mouse NCAPD3 were tested for knockdown of NCAPD3
271 protein by generating stable immortalized B6 mouse macrophage cell lines (40) transduced with isopropyl β-D-
272 1-thiogalactopyranoside (IPTG)-inducible shRNA lentiviral constructs (pLKO-puro-IPTG-3xLacO; Sigma;
273 **Supplemental Table 1**). Expression of the shRNA was induced by adding 2 mM IPTG to the cell culture medium
274 for 1-3 days. NCAPD3 protein levels relative to a loading control (Na/K ATPase) were determined by
275 densitometric analysis of cell lysate immunoblots using ImageJ software (41). Degree of knockdown was
276 determined by comparison to cells expressing a non-targeting shRNA treated with IPTG (**Fig. S1A**).

277 CRISPR/Cas targeting was used to insert a NCAPD3-targeting shRNA and green fluorescent protein
278 (GFP) expression cassette into the safe harbor locus of Col1a1 (42). A guide sequence, Col1a1 607/rev
279 (CAGGCCTCAGGTCTGCAGCA), that directs cutting near the PstI site downstream of the Col1a1 3'-UTR, was
280 validated using the Guide-it Complete sgRNA Screening System (Clontech) against a genomic target amplified
281 from B6SJL/F1 DNA. Large-scale preparations of Col1a1 607/rev sgRNA and Cas9 nuclease were ordered from
282 PNABio and prepared as directed.

283 A targeting vector, incorporating 1 kb 5' and 3' arms of homology from Col1a1, was designed to insert
284 the NCAPD3-targeting shRNA expression cassette at the position of the double-strand break directed by the
285 guide. The NCAPD3-targeting shRNA cassette was closely modeled on the cTGM vector from the Scott Lowe
286 laboratory (43), but without the elements required for embryonic stem cell selection. The vector was designed
287 using VectorBuilder.com and ordered as a large-scale supercoiled preparation (VectorBuilder). Aliquots of the
288 vector were spin clarified twice through Ultrafree-MC filters (Millipore).

289 Mixtures of Cas9 nuclease, sgRNA, and vector were prepared in Nuclease Free water (Qiagen) and
290 injected into the pro-nuclei of 0.5 dpc B6SJL/F2 fertilized oocytes. The mixtures, in ng/μl of Cas9/sgRNA/vector,
291 ranged from 20/20/2 to 5/5/0.5. Injected embryos were allowed to recover and surgically transferred through the

292 oviduct into 0.5 dpc CD1 pseudo-pregnant recipients. The resulting 78 pups were transferred at weaning from
293 the Case Transgenic and Targeting facility (Case Western Reserve University) to the principal investigator's
294 laboratory at the Cleveland Clinic.

295 The F_0 founders (both males and females) were initially screened by PCR for the presence of the
296 NCAPD3-targeting shRNA expression cassette using primers internal to the targeting vector. The correct
297 targeting of cassette-positive animals was then verified by LR-PCR using external and internal primers on both
298 sides and verified by sequencing of the LR-PCR products. Selected correctly targeted males and females were
299 back crossed to wild-type mice to generate three founder lines (**Fig. S1B**). These lines were crossed to
300 transgenic mice with villin-1 regulatory elements driving expression of an optimized reverse tetracycline-
301 controlled transactivator protein (rtTA*M2) (Jackson Labs strain#031285; B6;SJL-Tg(Vil1-rt-TA*M2)5Stang/J) to
302 result in a strain with tetracycline/doxycycline-inducible expression of the NCAPD3-targeting shRNA cassette in
303 the intestinal epithelium. These double-transgenic lines (NCAPD3 KD mice) were backcrossed 5-7 generations
304 onto a C57BL/6J strain background (Jackson Labs strain#000664), alternating male and female backcross
305 partners. Carriage of NCAPD3-targeting shRNA expression cassette and villin-rtTA*M2 transgene determined
306 by a real-time TaqMan PCR using custom 3 probe panel (Transnetyx Inc.). As the phenotypes of the three
307 NCAPD3 KD lines were similar, results from all three lines were combined in the data presented.

308 NCAPD3 knockdown was induced through daily intraperitoneal (i.p.) injection of 25 mg/kg 9-tert-butyl
309 doxycycline HCl (9-TB-dox; Echelon Biosciences, cat# B-0801). Expression of the transgene cassette was
310 monitored routinely by detection of GFP-expressing tissues using a handheld UV light source or IVIS Spectrum
311 CT small animal imager (PerkinElmer). NCAPD3 protein knockdown was confirmed by immunofluorescent
312 confocal microscopy and immunoblot of flow-sorted intestinal epithelial cells.

313

314 *Immunofluorescent staining of intestinal tissues*

315 Slides with tissue sections 8-10 μm thick were prepared from fresh frozen tissue embedded in OCT. After thawing
316 at room temperature for 15-30 minutes, slides were incubated in ice cold methanol for 10 minutes, followed by
317 three washes in phosphate buffered saline (PBS) for 5 minutes each on a shaker. Slides were incubated in
318 blocking buffer (5% human serum albumin/PBS) in a humid chamber at room temperature for 30-60 minutes.

319 Tissue sections were then incubated with NCAPD3 antibody (Bioss, cat# bs-7734R, 1:100 dilution) in blocking
320 buffer overnight at 4°C. Slides were washed three times in PBS, and goat anti-mouse IgG conjugated to Alexa
321 Fluor 488 (ThermoFisher, cat# A11001) diluted in blocking buffer was added. Slides were placed in a dark humid
322 chamber for one hour and then washed three times with PBS. Coverslips were mounted with Vectashield with
323 DAPI (Vector Labs) and sealed with nail polish. Images were obtained using a Leica TCS-SP8-AOBS confocal
324 microscope equipped with LAS-X software (Leica Microsystems).
325
326 *Flow cytometry enrichment of intestinal epithelial cells*
327 Mice were treated daily for 4 days with 25 mg/kg 9-TB-dox, (i.p.). Colons were removed, filleted open, and
328 washed three times with ice-cold phosphate-buffered saline (PBS). Tissue was incubated on ice for 20 min in 30
329 mM EDTA/ 1.5 mM DTT. Tissue was then transferred to 30 mM EDTA and incubated at 37°C for 10 min.
330 Epithelial cells were dislodged from bulk tissue by shaking, as previously described (44, 45). Cells were pelleted
331 by centrifugation at 100 x g for 3 min at 4°C, washed with ice-cold PBS, and pelleted again. Cells were incubated
332 in PBS with 8 mg/ml dispase (Gibco cat# 17105-041) and 5 mg/ml DNase (Worthington, cat# LS002007) at 37°C
333 for 20 min. Additional PBS was added, cells were passed through a 70 µm cell strainer, and then pelleted at 100
334 x g at 4°C for 3 min. Cells were resuspended in LIVE/DEAD Fixable Violet Dead Cell Stain (ThermoFisher cat#
335 L34964) and incubated at 4°C for 20 min. Cells were washed with ice-cold PBS and centrifuged at 100 x g at
336 4°C for 3 min. Stained cells were incubated with FcR blocking reagent (Miltenyi Biotec cat#130-092-575) for 5
337 min at 4°C and then subsequently stained with APC-conjugated anti-CD45 (1:200, Biolegend, Cat#109814) and
338 PE-conjugated anti-EpCAM/CD326 (1:50, ThermoFisher cat# 12-5791-83) at 4°C for 30 min. Cells were washed
339 with PBS/ 1 mM EDTA/ 0.5% BSA and pelleted at 100 x g at 4°C for 3 min. Cells were resuspended in PBS/ 2
340 mM EDTA/ 2% FBS, passed through a 35 µM filter, and sorted on a Bigfoot Spectral Cell Sorter (ThermoFisher)
341 for the collection of viable $CD45^-$ /$Epcam^+$ epithelial cells, further categorized by GFP expression. Gating strategy
342 shown in **Fig. S2**.
343
344 *Dextran sodium sulfate colitis model*

345 For colitis experiments, 7-11 week old male and female mice were randomized into treatment groups with
346 littermates distributed between treatment groups whenever possible. Mice were i.p. injected with 9-TB-dox (25
347 mg/kg) daily beginning 4 days prior to colitis induction and throughout the experiment. Colitis was induced over
348 7 days through the addition of 1.5% dextran sulfate sodium (DSS; 36,000–50,000 m.w., MP Biomedicals, LLC)
349 to the drinking water. Mice were monitored daily to calculate a disease activity index score (DAI; **Table S2**) and
350 sacrificed on day 7 for harvest of blood and tissues. Serum amyloid A (SAA) levels were measured from plasma
351 by ELISA (Immunology Consultants Laboratory). Portions of terminal ileum and proximal, transverse and distal
352 colon were fixed in 10% neutral buffered formalin for histologic analyses. Hematoxylin and eosin-stained sections
353 were evaluated blinded to treatment group and genotype to determine a colitis score (**Table S3**). Distal colon
354 segments were collected for analysis of cytokines/chemokines.
355
356 *Salmonella colitis model*
357 For colitis experiments, 7-11 week old male and female mice were randomized into treatment groups based on
358 genotype with littermates distributed between treatment groups whenever possible. Mice were i.p. injected with
359 9-TB-dox (25 mg/kg) every 24 hours beginning 4 days prior to infection and throughout the experiment. Twenty-
360 four hours prior to infection, mice were orally gavaged with 20 mg streptomycin. *Salmonella enterica*
361 Typhimurium ΔAroA SL3261 (gift from Bobby Cherayil, Department of Pediatrics, Harvard Medical School,
362 Boston, MA) was grown at 37°C with shaking in LB Miller broth supplemented with 50 µg/ml streptomycin. For
363 infections, a stationary culture diluted in PBS was used. Food was withdrawn for 4 hours prior to oral gavage
364 with $3x10^7$ cfu *Salmonella enterica* Typhimurium ΔAroA SL3261 in 100 µl of PBS. Mice were weighed and
365 monitored daily and sacrificed on day 7 for harvest of blood and tissues. A gross evaluation of diarrhea and
366 tissue damage was taken during dissection using a modified diarrhea score (46) (**Table S4**). SAA levels were
367 measured from plasma by ELISA (Immunology Consultants Laboratory). For bacterial enumeration, tissues
368 (liver, spleen, mesenteric lymph nodes (MLN), cecum, and colon) and stool were collected in 1 ml of sterile PBS,
369 stored on ice, and homogenized with an Omni Tissue Homogenizer (Omni International). Homogenized tissues
370 were serially diluted and plated onto LB agar plates containing 50 µg/ml streptomycin and incubated overnight
371 at 37°C. Calculated CFUs were then normalized to the weight of the tissue to obtain CFU/g. Portions of the

372 terminal ileum, cecum, and proximal and distal colon were fixed in 10% neutral buffered formalin for histological
373 analyses. Hematoxylin and eosin-stained sections were evaluated to determine the histopathology score (47)
374 (**Table S5**).
375
376 *Intestinal permeability assays*
377 For the determination of intestinal permeability by small molecule tracer flux *in vivo*, mice were food-restricted
378 for 3 hours prior to oral gavage with 12 mg fluorescein isothiocyanate-dextran (FITC; average MW: 3000-5000,
379 Sigma Aldrich) suspended in 100 µL sterile water. Blood was collected 2 hours post-gavage, and serum was
380 separated by centrifugation for 5 min at 5,000 rpm. Plasma was diluted in PBS and fluorescence determined at
381 530 nm with excitation at 485 nm. Measurement of intestinal permeability by flagellin bioassay was performed
382 by adding diluted plasma in duplicate to HEKBlue-mTLR5 reporter cells (InVivoGen) plated at 2.5 x10^4 cells/well
383 in 96-well plates for 24 hours. Cell culture supernatants were assayed for secreted alkaline phosphatase using
384 QUANT-Blue (InVivoGen) solution at 37°C for 3 hours.
385
386 *Quantification of cytokines/chemokines from intestinal tissue*
387 Colon and cecal tissues were manually homogenized in lysis buffer (20 mM Tris pH 7.5, 150 mM NaCl, 1mM
388 EDTA, 1mM EGTA, 1% Triton X100) with phosphatase and protease inhibitors (Sigma). Protein in the tissue
389 homogenates was quantified using a BCA assay (Pierce) and normalized to 25 µg/well. Multiplexed cytokine
390 and chemokine analysis was performed using the Proinflammatory Panel 1 (mouse) and Cytokine Panel 1
391 (mouse) kits from Meso Scale Diagnostics (MSD; Cat #K15048D, #K15245D) following the manufacturer's
392 instructions. The panels included the following analytes: IFN-γ, IL-1β, IL-2, IL-4, IL-5, IL-6, KC/GRO, IL-10, IL-
393 12p70, TNF-α, IL-9, MCP-1, IL-33, IL-27p28/IL-30, IL-15, IL-17A/F, MIP-1α, IP-10, MIP-2. Data was analyzed
394 using the MSD software, MSD Discovery Workbench 4.0.
395
396 *Immunoblots*
397 For analysis of NCAPD3 protein expression level, cells were lysed in Laemmli buffer (310 mM Tris pH 6.8, 25%
398 glycerol, 5% SDS, 715 mM 2-mercaptoethanol, 125 mg/mL bromophenol blue) on ice. The resulting lysate was

399 separated by SDS-PAGE and proteins transferred to a PVDF membrane using an iBlot2 transfer system
400 (Invitrogen). Membranes were blocked in 5% milk/Tris-buffered saline with 0.1% Tween-20 (TBST) and then
401 probed with primary antibodies (anti-CAPD3, Bethyl, A300-604A 1:1000, or anti-α-Tubulin, Sigma, T9026,
402 1:20,000) overnight at 4°C. After washing with TBST, blots were probed with HRP-conjugated secondary
403 antibodies (Jackson Laboratories) for 1 hour in 2.5% milk/TBST. Blots were developed by enhanced
404 chemiluminescence (Millipore). Uncropped blots used in figures shown in **Fig. S5**.
405
406 *Antibiotic testing of 9-TB-Dox*
407 To determine the antimicrobial effects of 9-TB-dox, log phase *Salmonella enterica* serovar Typhimurium ΔAroA
408 SL3261 cultures were diluted into LB medium with the indicated concentrations of 9-TB-dox or doxycycline in
409 96-well plates in triplicate. Bacterial growth over time at 37°C was monitored by absorbance at 600 nm in a
410 BioTek Synergy H1 plate reader.
411
412 *Quantitative Real Time PCR (qRT-PCR)*
413 Total RNA was isolated using Trizol (ThermoFisher) from total cecal tissue homogenates, per manufacturer's
414 instructions. RNA was converted to cDNA using iScript cDNA synthesis kit (BioRad), containing 1 µg RNA per
415 reaction. Transcript levels were measured by qPCR (see **Table S6** for primer information) in duplicate using
416 SYBR Green supermix (BioRad) and quantified using the $2^{-\Delta\Delta CT}$ method.
417
418 *Statistical Analysis*
419 Statistical analyses were performed using GraphPad Prism software (version 10). Groups were compared by
420 unpaired 2-tailed t-test or one-way ANOVA with *post-hoc* Sidak's multiple comparisons test. Differences were
421 considered significant when $p<0.05$. Specific tests used for each dataset are detailed in the figure legends.
422
423 *Data Availability*
424 All relevant data are publicly available within the manuscript and its supporting information files.
425

426 **Acknowledgments**

427 We thank David LePage and Ron Conlon in the Case Transgenic & Targeting Facility for their guidance, design,
428 and generation of the targeted NCAPD3KD mouse founders. We appreciate the assistance of Dr. Kewal
429 Asosingh and the expertise of Cleveland Clinic Research Flow Cytometry Core Facility (RRID:SCR_026460) in
430 optimization of the isolation and analysis of intestinal epithelial cells. We also thank Apryl Helmick in the
431 Cleveland Clinic Research Histology Core for patiently processing all our mouse tissues. We are very
432 appreciative of the technical support and guidance from members of the McDonald laboratory, Andràs Ponti, Lily
433 Markley, and Isabella Willis, as well as Dr. Kim Such and Tori Evans from the Biological Resources Unit. We
434 thank Dr. Bobby Cherayil for the gift of the *Salmonella* ΔAroA strain. We especially thank Dr. Serpil Erzurum for
435 her timely support of this project and ongoing support of our research programs.

436

437 **Figure Legends**

438 **Figure 1: Design and characterization of NCAPD3KD mice. A.** Schematic of transgenic targeting cassette
439 and genomic insertion strategy. **B.** Intestinal expression of transgene cassette confirmed by fluorescent imaging
440 of intestinal tissues *ex vivo*. Mice were injected with saline (Control) or 9-TB-Dox (25 mg/kg ip) for 4 days. Tissues
441 were excised and imaged on an IVIS small animal imager. **C.** Visualization of NCAPD3 knockdown in colonic
442 tissue by immunofluorescent confocal microscopy. Mice were treated with 9-TB-Dox (25 mg/kg; i.p. daily) for 2
443 days, and intestinal tissues were excised. Induction of transgene cassette visualized by detection of GFP reporter
444 gene (green), NCAPD3 (red), and nuclei stained with DAPI (grey). Slides imaged with 10x objective. **D.** Larger
445 image presentation of NCAPD3 (red) and GFP (green) colonic expression of 9-TB-Dox treated mice from C to
446 visualize the non-overlapping signals of NCAPD3 and GFP in the colon epithelium. Nuclei stained with DAPI
447 (blue). **E.** Quantification of intestinal epithelial NCAPD3 levels by immunoblot. Intestinal epithelial cells were
448 isolated from mice treated with 9-TB-Dox (25 mg/kg i.p.) for 4 days, and $Epcam^{+}$ /$CD45^{-}$ cells were sorted via
449 flow cytometry for GFP positivity. NCAPD3 protein levels were assessed by immunoblotting relative to a tubulin
450 loading control and quantified using ImageJ.

451

452 **Figure 2: Intestinal epithelial NCAPD3 knockdown does not result in spontaneous colitis.** Mice were
453 treated with saline or 9-TB-Dox (25 mg/kg i.p.) daily for 10 days (n=5 mice/group). **A.** Weight change relative to
454 starting weight. **B.** Gross evaluation of colonic pathology at endpoint. **C.** Histopathology of distal colon tissue. **D.**
455 Intestinal barrier integrity assessed by plasma bioassay on HEKBlue-mTLR5 reporter cell line. **E.** Systemic
456 inflammation assessed by quantification of SAA at endpoint. Mean ±SEM graphed. Significance determined by
457 unpaired 2-tailed t-test.
458
459 **Figure 3: Knockdown of NCAPD3 expression in intestinal epithelial cells sensitizes mice to intestinal**
460 **injury with dextran sodium sulfate.** NCAPD3 KD mice (n=16-18 mice/group) were treated daily with either
461 saline or 9-TB-Dox (25 mg/kg i.p.) 4 days prior to 1.5% DSS administration for 7 days. **A.** Weight change during
462 DSS treatment. **B.** Disease activity index during DSS treatment. **C.** Evaluation of distal colon histopathology
463 using a validated colitis scoring system. **D.** Paracellular intestinal permeability monitored by serum fluorescence
464 levels 2 hours after 4 kDa FITC-dextran gavage (12 mg/mouse; n=4 mice/group). **E.** Measurement of intestinal
465 permeability by flagellin bioassay using endpoint serum samples (n=4 mice/group). **F.** Systemic inflammation
466 evaluated by SAA levels. Mean± SEM graphed. Significance determined by 2-way ANOVA with Sidak's multiple
467 comparisons test (A. & B.) or 2-tailed unpaired t-test (C.-F.).
468
469 **Figure 4: NCAPD3 KD mice are more susceptible to intestinal damage from *Salmonella* Typhimurium**
470 **infection.** NCAPD3 KD mice (KD) and mice that lacked the villin-rtTA transgene (C) were treated daily with 9-
471 TB-Dox (25 mg/kg) for 4 days prior to oral antibiotic treatment and subsequent oral infection with *Salmonella*
472 *enterica* serovar Typhimurium ΔAroA (n=25-28 mice/group). **A.** Weight change after *Salmonella* infection
473 (p=0.0145). **B.** Tissue and stool bacterial loads. **C.** Endpoint gross diarrhea score. **D.** Endpoint histopathology
474 score. **E.** Cecal transcript levels of antimicrobial peptides. Transcripts were normalized to 18S and graphed
475 relative to the mean of control (C) mice. Mean ±SEM graphed. Significance determined by 2-way ANOVA with
476 Sidak's multiple comparisons test (A.-D.) or unpaired 2-tailed t-test (E.).
477
478 **References**

479 1. Peterson LW, Artis D. Intestinal epithelial cells: regulators of barrier function and immune homeostasis.
480 Nat Rev Immunol. 2014;14(3):141-53.
481 2. Okumura R, Takeda K. Roles of intestinal epithelial cells in the maintenance of gut homeostasis. Exp
482 Mol Med. 2017;49(5):e338.
483 3. Suzuki T. Regulation of intestinal epithelial permeability by tight junctions. Cell Mol Life Sci.
484 2013;70(4):631-59.
485 4. Roda G, Sartini A, Zambon E, Calafiore A, Marocchi M, Caponi A, et al. Intestinal epithelial cells in
486 inflammatory bowel diseases. World J Gastroenterol. 2010;16(34):4264-71.
487 5. Liu TC, Stappenbeck TS. Genetics and Pathogenesis of Inflammatory Bowel Disease. Annu Rev
488 Pathol. 2016;11:127-48.
489 6. Shu L, Zhang H. Condensin complexes: from chromatin organization to disease. Nucleus.
490 2026;17(1):2626198.
491 7. Rodemoyer B, Kariyawasam G, Subramanian V, Schmidt K. Condensin II interacts with BLM helicase
492 in S phase to maintain genome stability. Commun Biol. 2025;8(1):492.
493 8. Ward JR, Vasu K, Deutschman E, Halawani D, Larson PA, Zhang D, et al. Condensin II and GAIT
494 complexes cooperate to restrict LINE-1 retrotransposition in epithelial cells. PLoS Genet.
495 2017;13(10):e1007051.
496 9. Deutschman E, Ward JR, Kumar A, Ray G, Welch N, Lemieux ME, et al. Condensin II protein
497 dysfunction impacts mitochondrial respiration and mitochondrial oxidative stress responses. J Cell Sci.
498 2019;132(22).
499 10. Longworth MS, Walker JA, Anderssen E, Moon NS, Gladden A, Heck MM, et al. A shared role for
500 RBF1 and dCAP-D3 in the regulation of transcription with consequences for innate immunity. PLoS Genet.
501 2012;8(4):e1002618.
502 11. Schuster AT, Homer CR, Kemp JR, Nickerson KP, Deutschman E, Kim Y, et al. Chromosome-
503 associated protein D3 promotes bacterial clearance in human intestinal epithelial cells by repressing
504 expression of amino acid transporters. Gastroenterology. 2015;148(7):1405-16.e3.

505 12. Martin CA, Murray JE, Carroll P, Leitch A, Mackenzie KJ, Halachev M, et al. Mutations in genes
506 encoding condensin complex proteins cause microcephaly through decatenation failure at mitosis. Genes Dev.
507 2016;30(19):2158-72.
508 13. Dawkins JB, Wang J, Maniati E, Heward JA, Koniali L, Kocher HM, et al. Reduced Expression of
509 Histone Methyltransferases KMT2C and KMT2D Correlates with Improved Outcome in Pancreatic Ductal
510 Adenocarcinoma. Cancer Res. 2016;76(16):4861-71.
511 14. Jing Z, Liu Q, He X, Jia Z, Xu Z, Yang B, et al. NCAPD3 enhances Warburg effect through c-myc and
512 E2F1 and promotes the occurrence and progression of colorectal cancer. J Exp Clin Cancer Res.
513 2022;41(1):198.
514 15. Ma Y, Du J, Chen M, Gao N, Wang S, Mi Z, et al. Mitochondrial DNA methylation is a predictor of
515 immunotherapy response and prognosis in breast cancer: scRNA-seq and bulk-seq data insights. Front
516 Immunol. 2023;14:1219652.
517 16. Lu T, Yang J, Cai Y, Ding M, Yu Z, Fang X, et al. NCAPD3 promotes diffuse large B-cell lymphoma
518 progression through modulating SIRT1 expression in an H3K9 monomethylation-dependent manner. J Adv
519 Res. 2025;68:163-78.
520 17. Yang F, Zheng Y, Luo Q, Zhang S, Yang S, Chen X. Knockdown of NCAPD3 inhibits the tumorigenesis
521 of non-small cell lung cancer by regulation of the PI3K/Akt pathway. BMC Cancer. 2024;24(1):408.
522 18. Qu L, Che H, Zhao J, Lu X, Ren Z, Wu Y, et al. NCAPD3 is a prognostic biomarker and is correlated
523 with immune infiltrates in glioma. Histol Histopathol. 2024;39(11):1473-84.
524 19. Zhang SY, Luo Q, Xiao LR, Yang F, Zhu J, Chen XQ, et al. Role and mechanism of NCAPD3 in
525 promoting malignant behaviors in gastric cancer. Front Pharmacol. 2024;15:1341039.
526 20. Jiang D, Nelson ML, Gally F, Smith S, Wu Q, Minor M, et al. Airway epithelial NF-kappaB activation
527 promotes Mycoplasma pneumoniae clearance in mice. PLoS One. 2012;7(12):e52969.
528 21. Boller K, Arpin M, Pringault E, Mangeat P, Reggio H. Differential distribution of villin and villin mRNA in
529 mouse intestinal epithelial cells. Differentiation. 1988;39(1):51-7.
530 22. Grassl GA, Valdez Y, Bergstrom KS, Vallance BA, Finlay BB. Chronic enteric salmonella infection in
531 mice leads to severe and persistent intestinal fibrosis. Gastroenterology. 2008;134(3):768-80.

532 23. Michielan A, D'Incà R. Intestinal Permeability in Inflammatory Bowel Disease: Pathogenesis, Clinical
533 Evaluation, and Therapy of Leaky Gut. Mediators Inflamm. 2015;2015:628157.
534 24. Turpin W, Lee SH, Raygoza Garay JA, Madsen KL, Meddings JB, Bedrani L, et al. Increased Intestinal
535 Permeability Is Associated With Later Development of Crohn's Disease. Gastroenterology. 2020;159(6):2092-
536 100.e5.
537 25. Rudbaek JJ, Agrawal M, Torres J, Mehandru S, Colombel JF, Jess T. Deciphering the different phases
538 of preclinical inflammatory bowel disease. Nat Rev Gastroenterol Hepatol. 2024;21(2):86-100.
539 26. Chen R, Chen Q, Zheng J, Zeng Z, Chen M, Li L, et al. Serum amyloid protein A in inflammatory bowel
540 disease: from bench to bedside. Cell Death Discov. 2023;9(1):154.
541 27. Chhibba T, Gros B, King JA, Windsor JW, Gorospe J, Leibovitzh H, et al. Environmental risk factors of
542 inflammatory bowel disease: toward a strategy of preventative health. Journal of Crohn's and Colitis.
543 2025;19(4).
544 28. Sanchez-Munoz F, Dominguez-Lopez A, Yamamoto-Furusho JK. Role of cytokines in inflammatory
545 bowel disease. World J Gastroenterol. 2008;14(27):4280-8.
546 29. Ajuebor MN, Kunkel SL, Hogaboam CM. The role of CCL3/macrophage inflammatory protein-1α in
547 experimental colitis. European Journal of Pharmacology. 2004;497(3):343-9.
548 30. Godinez I, Keestra AM, Spees A, Bäumler AJ. The IL-23 axis in Salmonella gastroenteritis. Cellular
549 Microbiology. 2011;13(11):1639-47.
550 31. Bevins CL, Martin-Porter E, Ganz T. Defensins and innate host defence of the gastrointestinal tract.
551 Gut. 1999;45(6):911-5.
552 32. Ramasundara M, Leach ST, Lemberg DA, Day AS. Defensins and inflammation: the role of defensins
553 in inflammatory bowel disease. J Gastroenterol Hepatol. 2009;24(2):202-8.
554 33. Porter CK, Tribble DR, Aliaga PA, Halvorson HA, Riddle MS. Infectious gastroenteritis and risk of
555 developing inflammatory bowel disease. Gastroenterology. 2008;135(3):781-6.
556 34. Ray G, Longworth MS. Epigenetics, DNA Organization, and Inflammatory Bowel Disease. Inflamm
557 Bowel Dis. 2019;25(2):235-47.

558 35. Hadjur S, Williams LM, Ryan NK, Cobb BS, Sexton T, Fraser P, et al. Cohesins form chromosomal cis-
559 interactions at the developmentally regulated IFNG locus. Nature. 2009;460(7253):410-3.
560 36. Watanabe T, Ishihara K, Hirosue A, Watanabe S, Hino S, Ojima H, et al. Higher-order chromatin
561 regulation and differential gene expression in the human tumor necrosis factor/lymphotoxin locus in
562 hepatocellular carcinoma cells. Mol Cell Biol. 2012;32(8):1529-41.
563 37. Wang B, Bian Q. SATB1 prevents immune cell infiltration by regulating chromatin organization and
564 gene expression of a chemokine gene cluster in T cells. Commun Biol. 2024;7(1):1304.
565 38. Cai S, Lee CC, Kohwi-Shigematsu T. SATB1 packages densely looped, transcriptionally active
566 chromatin for coordinated expression of cytokine genes. Nat Genet. 2006;38(11):1278-88.
567 39. Crawford BI, Talley MJ, Russman J, Riddle J, Torres S, Williams T, et al. Condensin-mediated
568 restriction of retrotransposable elements facilitates brain development in Drosophila melanogaster. Nature
569 Communications. 2024;15(1):2716.
570 40. Spera I, Sánchez-Rodríguez R, Favia M, Menga A, Venegas FC, Angioni R, et al. The J2-Immortalized
571 Murine Macrophage Cell Line Displays Phenotypical and Metabolic Features of Primary BMDMs in Their M1
572 and M2 Polarization State. Cancers (Basel). 2021;13(21).
573 41. Schneider CA, Rasband WS, Eliceiri KW. NIH Image to ImageJ: 25 years of image analysis. Nature
574 Methods. 2012;9(7):671-5.
575 42. Beard C, Hochedlinger K, Plath K, Wutz A, Jaenisch R. Efficient method to generate single-copy
576 transgenic mice by site-specific integration in embryonic stem cells. genesis. 2006;44(1):23-8.
577 43. Dow LE, Premsrirut PK, Zuber J, Fellmann C, McJunkin K, Miething C, et al. A pipeline for the
578 generation of shRNA transgenic mice. Nature Protocols. 2012;7(2):374-93.
579 44. Gracz AD, Puthoff BJ, Magness ST. Identification, isolation, and culture of intestinal epithelial stem
580 cells from murine intestine. Methods Mol Biol. 2012;879:89-107.
581 45. Ge Y, Zadeh M, Mohamadzadeh M. Dissociation and flow cytometric isolation of murine intestinal
582 epithelial cells for multi-omic profiling. STAR Protoc. 2023;4(1):101936.
583 46. Woo H, Okamoto S, Guiney D, Gunn JS, Fierer J. A Model of Salmonella Colitis with Features of
584 Diarrhea in SLC11A1 Wild-Type Mice. PLOS ONE. 2008;3(2):e1603.

585 47. Barthel M, Hapfelmeier S, Quintanilla-Martínez L, Kremer M, Rohde M, Hogardt M, et al. Pretreatment
586 of mice with streptomycin provides a Salmonella enterica serovar Typhimurium colitis model that allows
587 analysis of both pathogen and host. Infect Immun. 2003;71(5):2839-58.

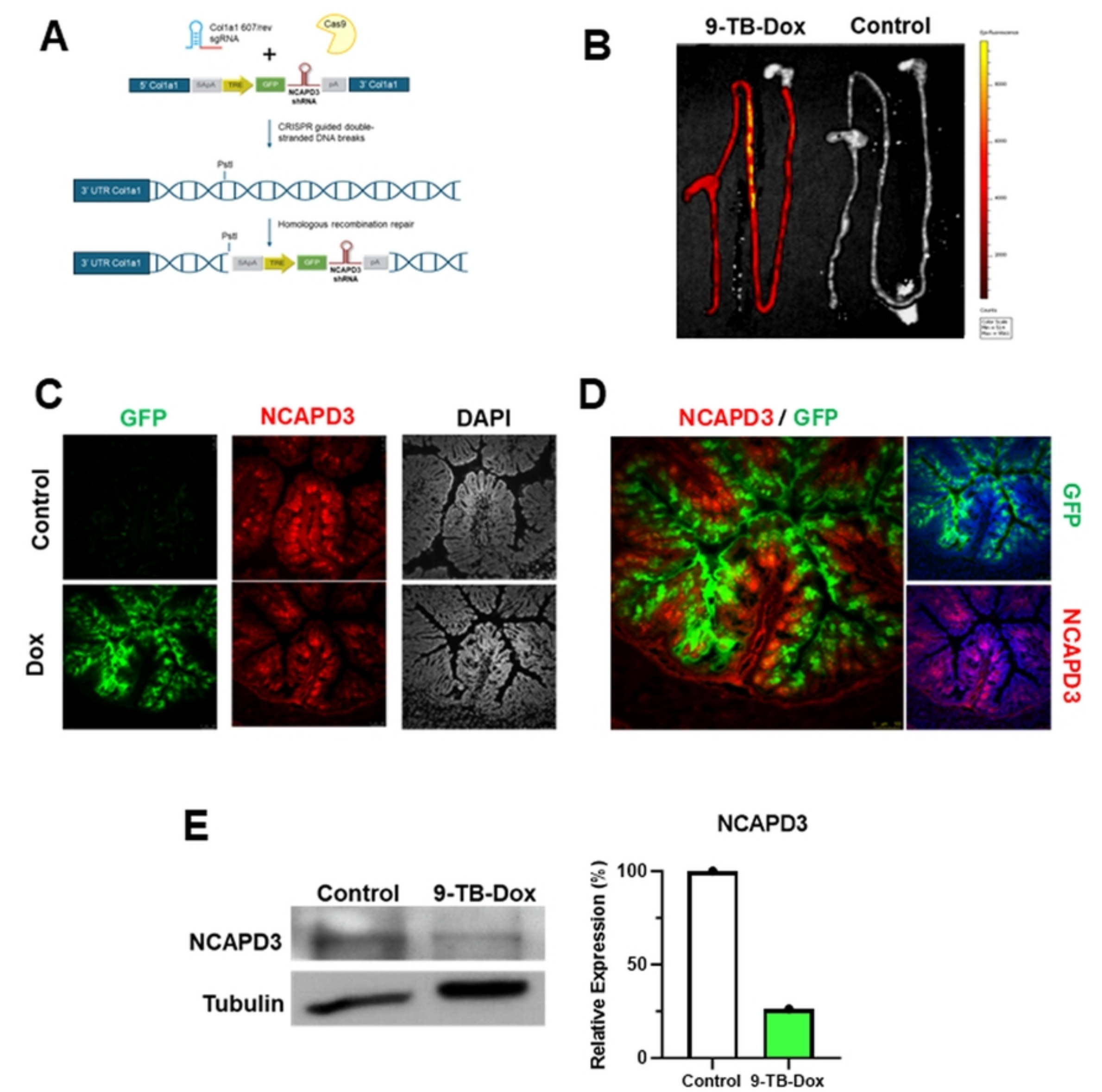

Figure 1

Figure 1

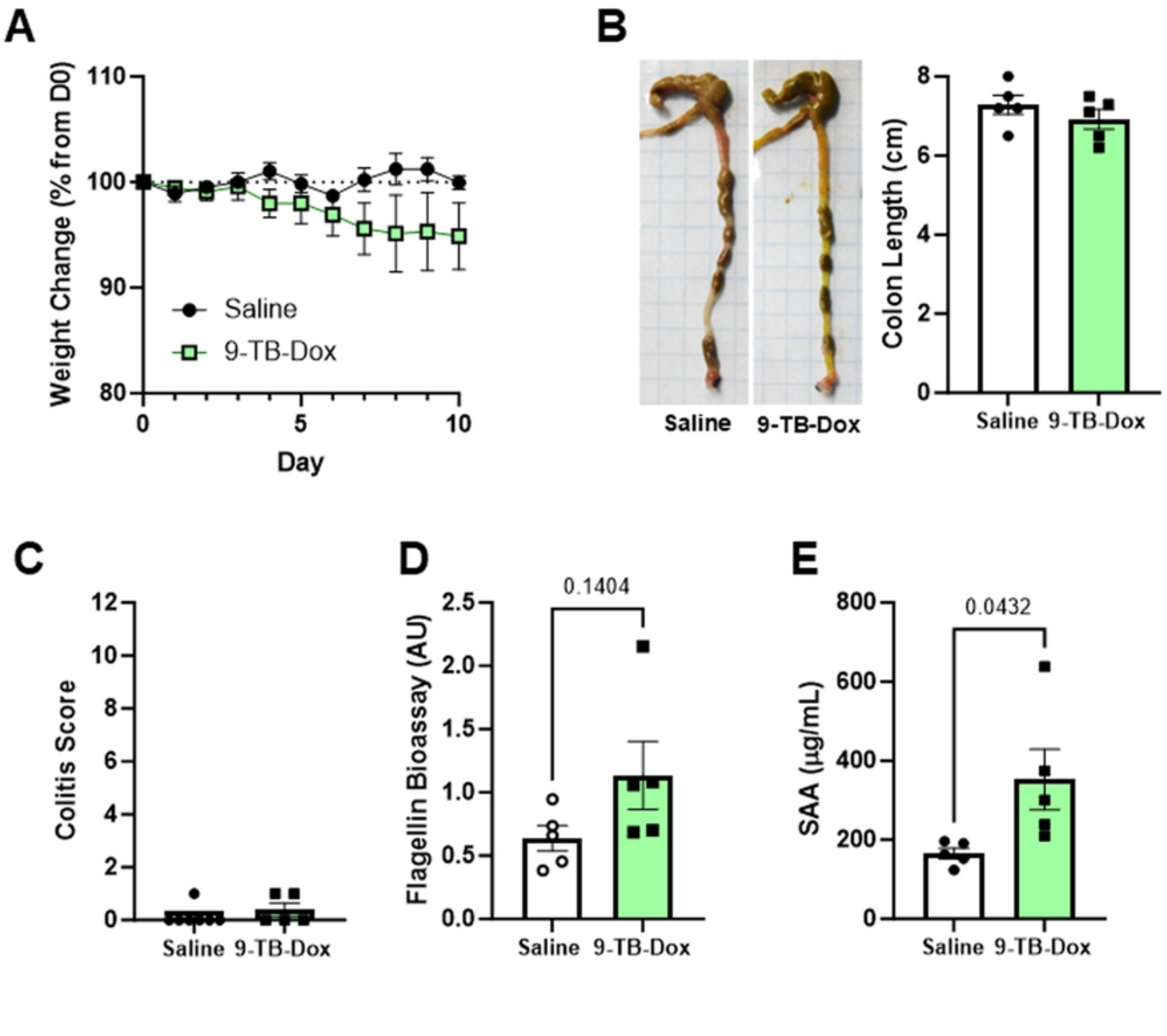

Figure 2

Figure 2

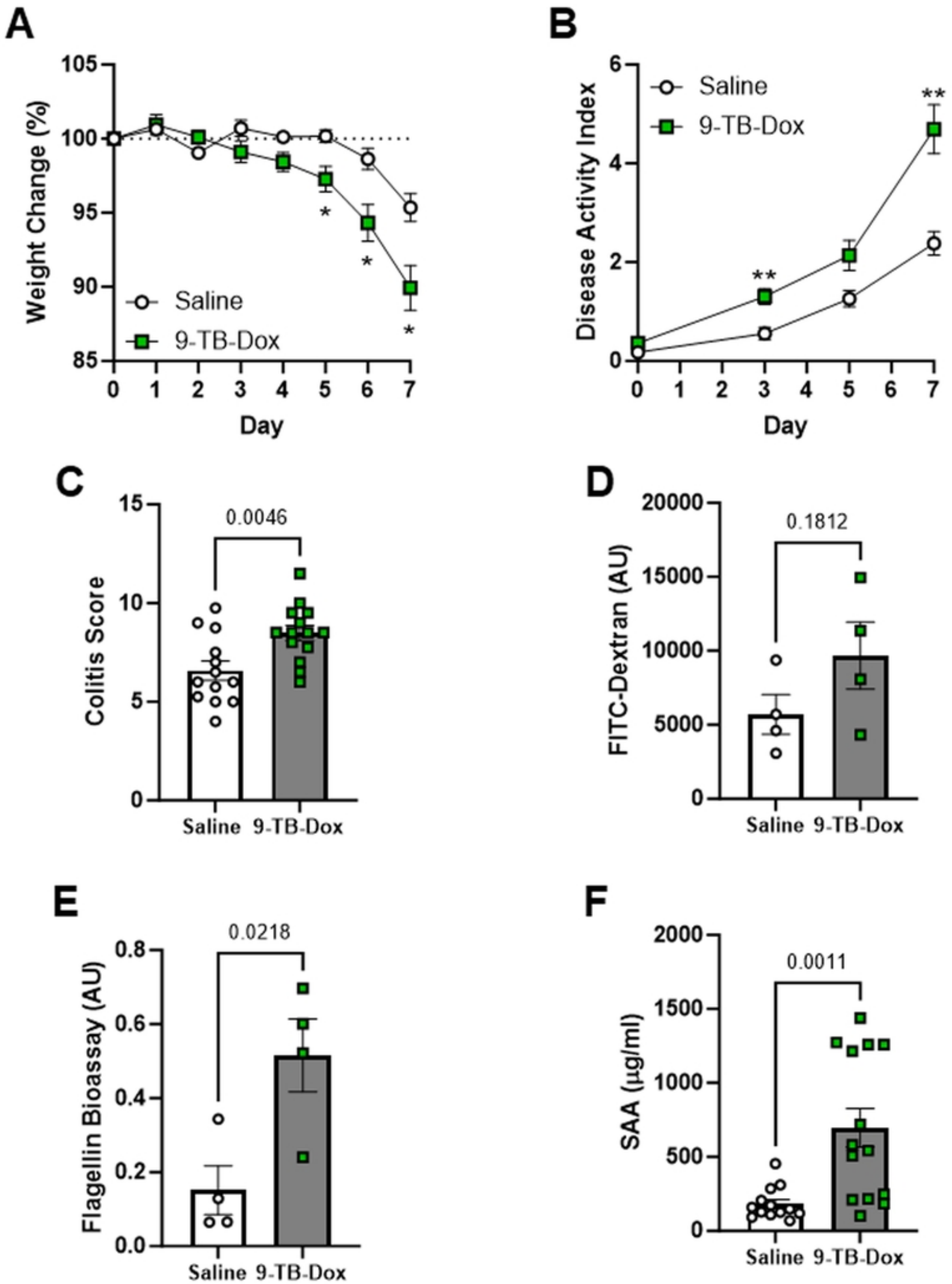

Figure 3

Figure 3

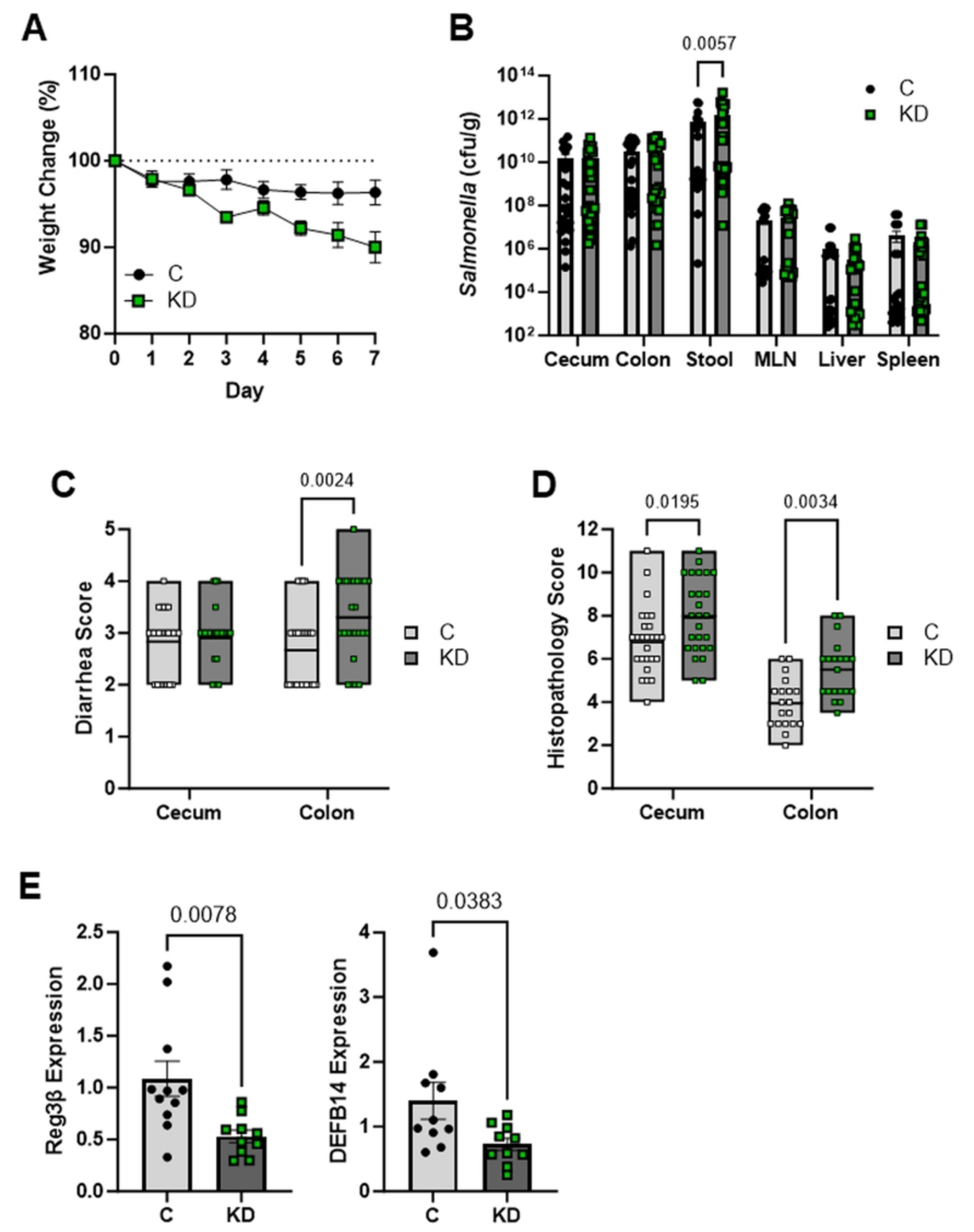

Figure 4

Figure 4